Research in Astron. Astrophys. **2010** Vol. **10** No. **8**, 777–784
http://www.raa-journal.org *http://www.iop.org/journals/raa*

***R**esearch in*
***A**stronomy and*
***A**strophysics*

Radiation-driven implosion in the Cepheus B molecular cloud

Sheng Chen[1,2] and Maohai Huang[1]

[1] National Astronomical Observatories, Chinese Academy of Sciences, Beijing 100012, China; *mhuang@nao.cas.cn*
[2] Graduate University of Chinese Academy of Sciences, Beijing 100049, China

Received 2010 March 23; accepted 2010 April 28

Abstract We analyze large scale mapping observations of the molecular lines in the ^{12}CO ($J = 2 - 1$) , ^{12}CO ($J = 3 - 2$) , ^{13}CO ($J = 2 - 1$) , and ^{13}CO ($J = 3 - 2$) transition emissions toward the Cepheus B molecular cloud with the KOSMA 3m-telescope. The integrated intensity map of the ^{12}CO ($J = 2 - 1$) transition has shown a structure with a compact core and a compact ridge extended to the north-west of the core. The cloud is surrounded by an optically bright rim, where the radiation-driven implosion (RDI) may greatly change the gas properties. The intensities of the CO ($J = 3 - 2$) transition are higher than those of the CO ($J = 2 - 1$) transition along the rim area. We find characteristic RDI structure in position-velocity diagrams. Non-LTE large velocity gradient (LVG) model analysis shows that the density and temperature at the edge are higher than that in the center. Our results provide evidences that an RDI is taking place in the Cepheus B molecular cloud.

Key words: submillimeter — ISM: clouds — ISM: globules — stars: formation

1 INTRODUCTION

The association Cepheus OB3 is one of the youngest groups of early type stars associated with the HII region S155 (Sharpless 1959) at a distance of 0.7 kpc (Blaauw 1964). The observations in the ^{12}CO ($J = 1 - 0$) line have shown a few bright components named Cepheus A, B, C, D, E, and F (Sargent 1977, 1979). Of the six components, the hottest CO feature and abundant dust emission were detected in Cepheus B, which was surrounded by an arc-like optical HII region S155. The molecular cloud/HII region complex with such a morphology is called the bright rimmed cloud (BRC), where star formation activity can be triggered by the radiation-driven implosion (RDI) mechanism.

The radio continuum observations (Felli et al. 1978) by the Westerbork Synthesis Radio Telescope (WSRT) confirmed that the UV radiation from a bright O7 star created an arc-shaped ionization front which surrounded the Cepheus B molecular cloud. The observations of the H_2CO and recombination lines (Panagia et al. 1981) have suggested that the ionized material was flowing away at about 11 $\mathrm{km\ s^{-1}}$, and the ionization front was moving into the molecular cloud at a velocity of about 2 $\mathrm{km\ s^{-1}}$. ^{12}CO ($J = 3 - 2$) and ^{13}CO ($J = 2 - 1$) observations, together with the far-infrared analysis, showed that the cloud was externally heated and the edge of the cloud was compressed by the expansion of S155 (Minchin et al. 1992).

Beuther et al. (2000) observed the Cepheus B area at a large scale in the $J = 3 - 2$ and 2–1 transitions of ^{12}CO, ^{13}CO and C^{18}O with the KOSMA 3 m-telescope. Based on the volume densities derived from the PDR model, they found that Cepheus B was highly clumped and the volume of these clumps fills only 2%–4% of the whole cloud. Mookerjea et al. (2006) confirmed this with further observations of [C I] $^3P_2$ – $^3P_1$ and ^{12}CO ($J = 4 - 3$) . Based on the studies of protoplanetary disks, Getman et al. (2009) found a spatial-temporal gradient of young stars from the molecular core toward HD 217086, which identified HD 217086 as the primary ionizing source of the cloud.

Although a lot of efforts have been made to characterize the physical conditions of Cepheus B, the mechanism of star formation in this region is still not quite clear. We present an analysis of a larger scale observation of multiple CO lines, and discuss the RDI as the possible trigger of star formation in this region.

2 OBSERVATIONS

The observations were carried out with the 3 m KOSMA sub-millimeter telescope using the On-The-Fly mode in 2004 March. Mapping observations of CO were made at ^{12}CO ($J = 2 - 1$) (230.538 GHz), ^{12}CO ($J = 3-2$) (345.789 GHz), ^{13}CO ($J = 2-1$) (220.399 GHz), and ^{13}CO ($J = 3 - 2$) (330.588 GHz) transitions. The dual-channel 230/345 GHz SIS receivers (Graf et al. 1998) were used to simultaneously observe the two transitions of the isotopes. The system temperatures were about 160 K for $J = 2-1$ transitions and 300 K for $J = 3-2$ transitions. The pointing accuracy was better than 15″ and the angular resolutions (FWHM of the beam) were 130″ at 220 GHz and 80″ at 330 GHz. The efficiency of the telescope $F_{\rm eff}$ was 93%, and the main beam efficiencies of $B_{\rm eff}$ were 68% at 230 GHz and 72% at 345 GHz. Line intensities were converted on the main beam scale, using $T_{\rm mb} = (F_{\rm eff}/B_{\rm eff})T_A^*$ (Downes 1989).

For the ^{12}CO ($J = 2 - 1$) and ^{12}CO ($J = 3 - 2$) transition emissions, a 15×15 map was observed centered at RA=22$^{\rm h}$55$^{\rm m}$20.708$^{\rm s}$, DEC=62°20′ 00.02″ (B1950), while for ^{13}CO ($J = 2 - 1$) and ^{13}CO ($J = 3 - 2$) , a 12×11-point map was made centered at RA=22$^{\rm h}$55$^{\rm m}$24.000$^{\rm s}$, DEC=62°20′ 41.01″ (B1950). The grid spacing was 1′. Each point of the grid was observed 5–6 times with a total integration time of 2 min and the spectra were averaged in order to increase the signal to noise ratio. The observed data were reduced and plotted with CLASS and GREG of the Gildas package (Guilloteau & Lucas 2000). The CO ($J = 3 - 2$) transitions were smoothed to a resolution of 130″ to match the CO ($J = 2 - 1$) transitions.

3 RESULTS

The spectra of ^{12}CO ($J = 2-1$) , ^{12}CO ($J = 3-2$) , ^{13}CO ($J = 2-1$) , and ^{13}CO ($J = 3-2$) at the center positions of the observations are shown in Figure 1. The observed spectra show approximate Gaussian line shapes. From the four lines, the average $v_{\rm LSR}$ is -13.1 ± 0.1 km s^{-1}.

We have made integration intensity maps of the ^{12}CO ($J = 2 - 1$) line integrated from –18 to –8 km s^{-1}superimposed on the optical POSS2 red plate as shown in Figure 2. The O7 star HD 217086 and the B1 star HD 217061 of the Cepheus OB3 association are marked, and the former is thought to be the primary ionizing source of the cloud (Getman et al. 2009). The map shows a compact core and a compact ridge with a cometary shaped tail extended in the south-east direction. There is a steep drop-off in CO emission at the northern and western side of the cloud, forming a well-defined boundary edge. In addition, an optically bright rim is shown in the north-west direction as seen in the POSS2 red plate in gray scale. The compact ridge of the CO integrated intensity contours is surrounded by the bright rim. The average radial velocity of the Cepheus OB3 association is -14.5 ± 4.5 km s^{-1}(Garmany 1973, derived from optical spectra), while in the north-western part the $v_{\rm LSR}$ of our CO observation, it is also about –15 to –14 km s^{-1}(see Fig. 3). The agreement between optical and CO velocities confirms that the bright rim and the molecular cloud are physically

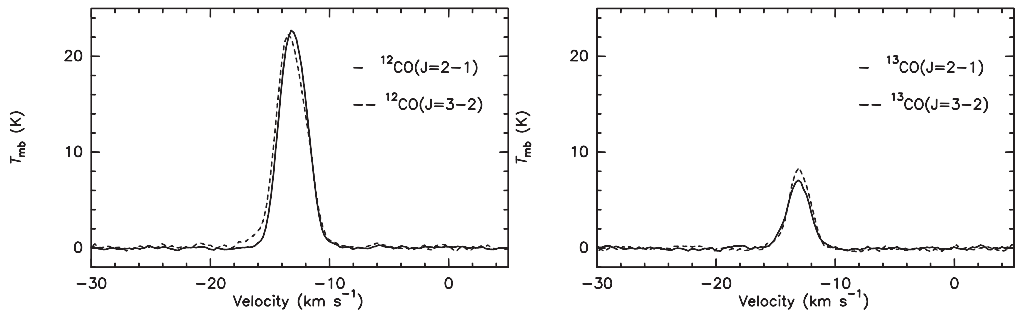

Fig. 1 Spectra at the center positions. The vertical axis is main beam temperature $T_{\rm mb}$, and the horizontal axis is the velocity. *Left panel*: ^{12}CO ($J = 2 - 1$ and $J = 3 - 2$); *Right panel*: ^{13}CO ($J = 2 - 1$ and $J = 3 - 2$). (Solid lines for $J = 2 - 1$ transitions and dashed lines for $J = 3 - 2$ transitions).

associated. The morphology of the cloud and the HII region matches well with the scenario of bright-rimmed clouds, which are possibly shaped by the radiation-driven implosion of the ionizing source (Bertoldi 1989).

In order to investigate the kinetic and physical conditions in this region, we take position A (offset 1, –1) at the center of the cloud and position B (offset –2, 1) at the edge, as marked in Figure 2. The line properties are compared in Table 1. At position B, the ^{12}CO ($J = 3 - 2$) transition intensity is higher than that of ^{12}CO ($J = 2 - 1$) , while at position A, the ^{12}CO ($J = 2 - 1$) transition intensity is higher than that of ^{12}CO ($J = 3 - 2$) . The reversed line ratio suggests higher density or higher temperature at position B. Further, we plot spectra of the ^{12}CO ($J = 3 - 2$) (red) over ^{12}CO ($J = 2 - 1$) (black) of all grid points in Figure 3. We can see that the A and B positions are not alone in this aspect. The ^{12}CO ($J = 3 - 2$) intensity is higher than the ^{12}CO ($J = 2 - 1$) intensity across the bright rim area for most grid positions, indicating the UV radiation is interacting with the molecular cloud and pumping molecules to higher excitation levels.

Table 1 ^{12}CO Line Parameters

Line	$v_{\rm LSR}$ (km s^{-1})	FWHM (km s^{-1})	$T_{\rm mb}$(K)
^{12}CO ($J = 2 - 1$) (A)	–12.6 (0.1)	2.8 (0.1)	24.2 (0.3)
^{12}CO ($J = 3 - 2$) (A)	–12.9 (0.1)	3.0 (0.1)	21.9 (0.4)
^{12}CO ($J = 2 - 1$) (B)	–13.7 (0.1)	2.4 (0.1)	14.8 (0.8)
^{12}CO ($J = 3 - 2$) (B)	–13.6 (0.1)	2.6 (0.1)	19.7 (1.0)

From Figure 3 we also find a spatial shift of $v_{\rm LSR}$ from the head (north-west) to the tail (south-east) of the cloud, which is clearly shown in position-velocity (PV) diagrams along the diagonal direction from north-west to south-east in Figure 4.

4 DISCUSSION

As seen in Figure 2, the observed molecular cloud is surrounded by an ionized bright rim facing the exciting source with a hot core close to the rim and a cometary shaped tail on the side opposite to the rim. This scenario matches the properties of a BRC well, which is modeled as externally illuminated, photo-evaporated and ablated into the elongated head-tail morphologies by UV radiation of OB stars (Reipurth 1983). The isolation and simple morphology of BRCs make them ideal environments to investigate the RDI (Bertoldi 1989) mode of star formation, where pressure from the ionization

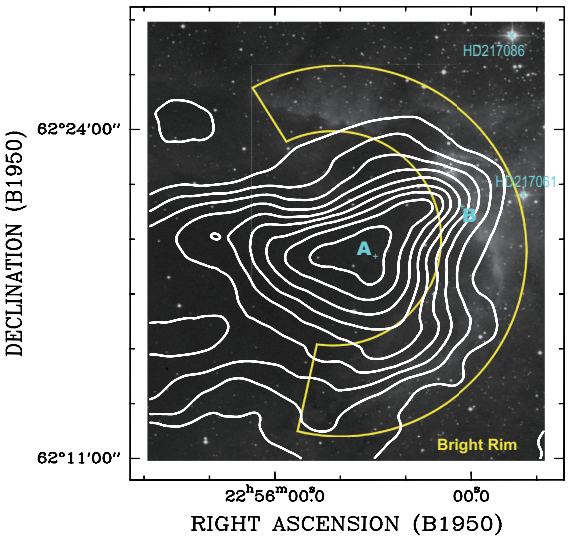

Fig. 2 Contours of the ^{12}CO ($J = 2-1$) line integrated intensity from –18 to –8 km s^{-1}(*white solid line*) overlaid on the POSS2 Red image (*gray scale*). The contour levels of solid lines are marked from 11 to 70 in steps of 7.4 km s^{-1}. Points A and B are marked as typical positions at the center (A) and the edge (B) of the cloud for further analysis. The bright rim in the optical image is marked in yellow. HD 217086 and HD 217061 are marked as blue crosses.

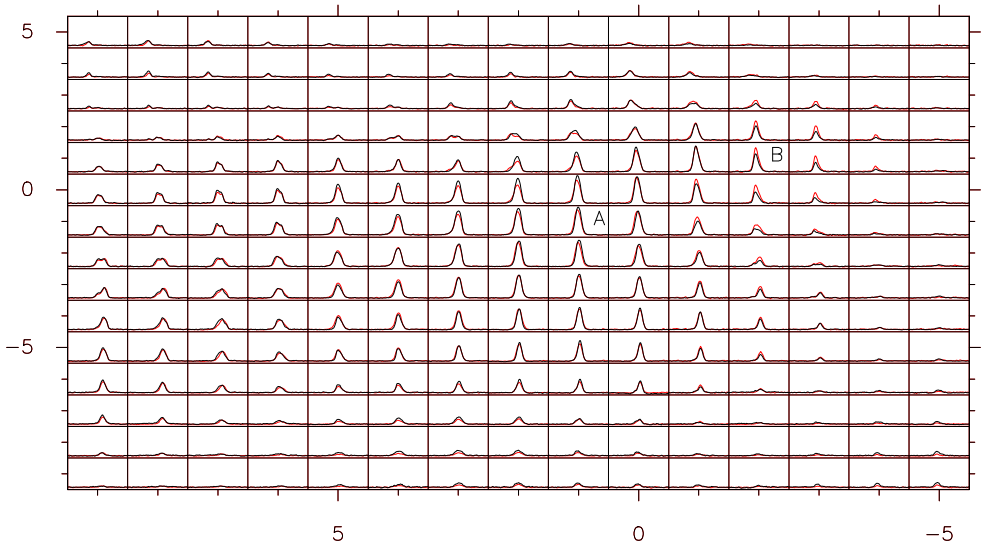

Fig. 3 Spectra of the ^{12}CO ($J = 2 - 1$) (*black*) and ^{12}CO ($J = 3 - 2$) (*red*) showing all grid points. For each grid point, the horizontal axis is the velocity with a scale from –30 to 5km s^{-1}, and the vertical axis is the main beam temperature from –2 to 25 K. A and B are the same positions as marked in Fig. 2.

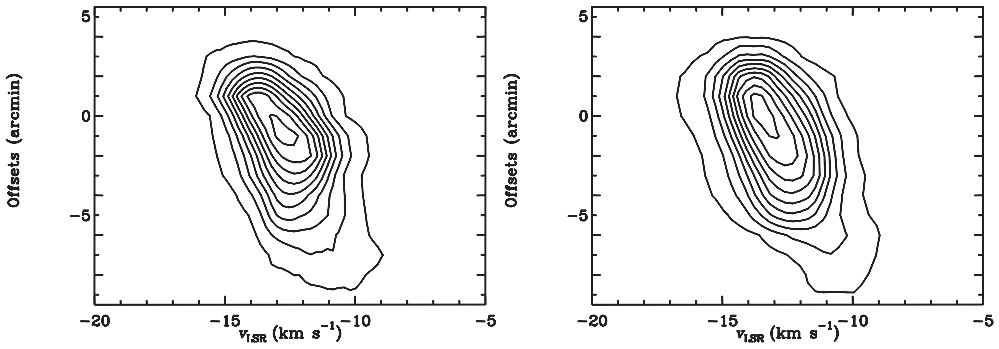

Fig. 4 P-V diagram constructed from the ^{12}CO ($J = 2 - 1$) (*left panel*) and ^{12}CO ($J = 3 - 2$) (*right panel*) along the diagonal direction from north-west (*positive offsets*) to south-east (*negative offsets*).

shock front at the surface propagates through a cloud and overcomes the magnetic, turbulent and thermal pressure, triggering cloud collapse, thereby also triggering local star formation.

In our case, the spatial shift of v_{LSR} shows strong connections with the RDI mechanism. The PV diagrams in Figure 4 show a velocity gradient from the head (north-west) of the cloud to the tail (south-east). The blueward elongation toward the head by about $3\,\mathrm{km\ s^{-1}}$from the center indicates that the head part is expanding toward us, while the redward elongation toward the tail by about $4\,\mathrm{km\ s^{-1}}$indicates the tail part is flowing away in the opposite direction. The velocity gradients of the head and tail match the RDI model prediction of Lefloch & Lazareff (1994), where the red-shift of the tail is caused by the acceleration of the gas across the tail, and the blue-shift of the head is because the compressed gas in the head moves faster than the gas immediately behind it. Such PV diagrams are reported by various BRC and cometary globule studies (Lefloch & Lazareff 1995; Sugitani 1997; White et al. 1997; Bachiller et al. 2002) which are explained by the RDI mechanism, and so are taken as a characteristic structure of the RDI.

The reversed line ratios across the bright rim are another interesting feature. The spatial distribution of the reversed line ratios suggest that they are physically connected with the RDI along the rim area. Higher transitions are more readily excited by higher temperatures or higher densities (Petitpas 1998), either of which can be a result of RDI. The highly luminous ionizing shock front from the RDI interacts with the molecular cloud, pumping more particles from a lower level to a higher one, which makes the $J = 3 - 2$ emission stronger along the rim area.

Table 2 Solutions of LVG Analysis

Position	N_{CO} (10^{16} cm^{-2})	n_{H_2} (10^4 cm^{-3})	T_{kin} (K)
A	3.2	1.6	40
	6.8	3.2	31
	10	4.0	31
	22	2.0	30
	46	1.0	30
	68	0.63	30
	100	0.20	32
B	1.1	4.0	71
	1.2	8.9	50
	1.3	50	45

In order to investigate RDI effects and their physical characteristics quantitatively, we made further analysis with a large velocity gradient (LVG, Goldreich et al. 1974; Qin et al. 2008a) radiative transfer model in the MIRIAD software package. In this model, the molecular cloud is considered spherically uniform and the non-LTE excitation properties are calculated based on the kinetic temperature ($T_{\rm kin}$), the column density per unit velocity interval ($N_{\rm CO}/\Delta V$), and the H_2 density ($n_{\rm H_2}$). In this case, we use the line intensity of ^{12}CO ($J = 2-1$) and the line ratio of ^{12}CO ($J = 3-2$) /^{12}CO ($J = 2-1$) to determine the volume density $n_{\rm H_2}$ and kinetic temperature $T_{\rm kin}$ at the two selected positions A and B, assuming the column density is in the range of 1×10^{14} to 1×10^{18} cm^{-2}, and $\Delta V = 1\,{\rm km\,s^{-1}}$. Representative solutions that can be fitted to the observations are listed in Table 2. A typical case is shown in Figure 5.

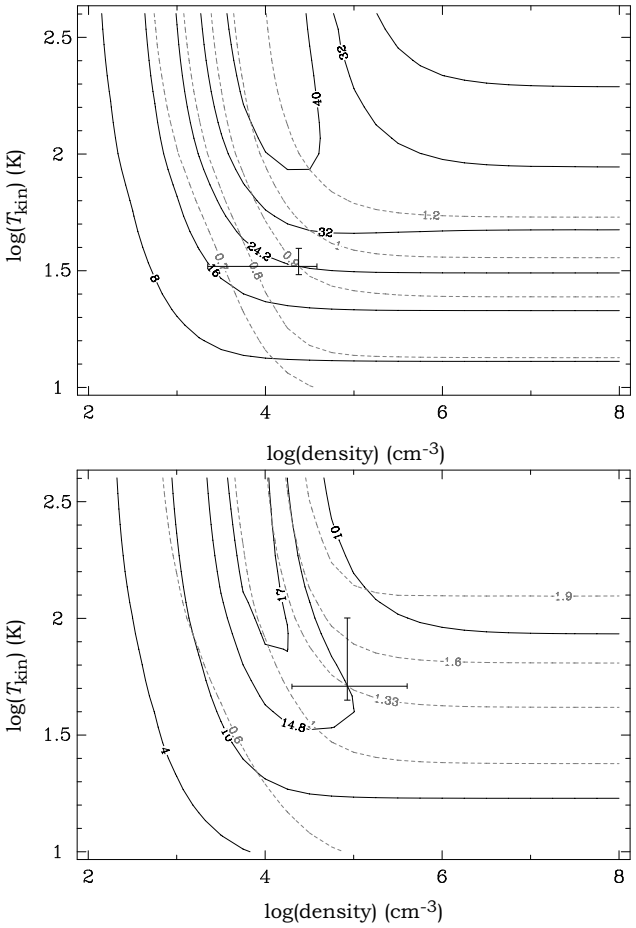

Fig. 5 LVG model analysis at position A ($N_{\rm CO} = 4.6 \times 10^{16}$ cm^{-2}, *upper panel*) and B ($N_{\rm CO} = 1.2 \times 10^{16}$ cm^{-2}, *bottom panel*) using the ^{12}CO ($J = 2-1$) and ^{12}CO ($J = 3-2$) line. The horizontal and vertical axes stand for volume density $n_{\rm H_2}$ and kinetic temperature $T_{\rm kin}$ in log scale, respectively. Solid curves are line intensity of ^{12}CO ($J = 2-1$) and dashed curves are the line ratios of ^{12}CO ($J = 3-2$) /^{12}CO ($J = 2-1$) . The results of $T_{\rm kin}$ and $n_{\rm H_2}$ are taken from the cross points of certain solid and dashed curves. The error bars indicate the range of possible solutions listed in Table 2.

For position A, various column densities are possible to explain the observation results self-consistently covering the range from 3×10^{16} to $1\times10^{18}\,\mathrm{cm}^{-2}$, with corresponding volume densities ranging from 0.2×10^{4} to $4.0\times10^{4}\,\mathrm{cm}^{-3}$. The average value of the possible volume densities is $2.0\times10^{4}\,\mathrm{cm}^{-3}$. For position B, the few self-consistent solutions require the column densities to be in a tiny range of 1.1×10^{16} to $1.3\times10^{16}\,\mathrm{cm}^{-2}$. The average density derived is $1.5\times10^{5}\,\mathrm{cm}^{-3}$, nearly one order of magnitude higher than that at position A. The average kinematic temperature of B (61 K) is also twice as high as that of A (32 K). Even in the cases that both positions have similar densities (e.g. $n_{\mathrm{H_2}}=4.0\times10^{4}\,\mathrm{cm}^{-3}$), the kinematic temperature required at position B is still 2.3 times higher than that at position A. Therefore, we can conclude that the reversed line ratios along the bright rim are produced by either high densities, or high temperatures, and likely both. Both possibilities can be explained by radiation and pressure of the ongoing RDI, where the ionizing shock wave of the RDI propagates into the molecular cloud, compressing it at the edge, and thus makes the density and temperature of the edge even higher than at the center.

In comparison with the LVG analysis results, we have also calculated the column densities assuming LTE conditions. Taking the upper energy level temperature of 16.6 K (Qin et al. 2008b), the column density of CO is given by (Garden et al. 1991):

$$N_{\mathrm{CO}}=1.08\times10^{13}\frac{T_{\mathrm{ex}}}{\exp(-16.6/T_{\mathrm{ex}})}\int T_{\mathrm{mb}}dv\,\mathrm{cm}^{-2}, \tag{1}$$

and

$$T_{\mathrm{ex}}=\frac{h\nu}{k}\left\{\ln\left\{1+\frac{h\nu}{k}\left[\frac{T_{\mathrm{mb}}}{f}+\frac{h\nu}{k}\left(\exp\left(\frac{h\nu}{kT_{\mathrm{bg}}}\right)-1\right)^{-1}\right]^{-1}\right\}\right\}^{-1}\ \mathrm{K}, \tag{2}$$

where the beam filling factor f is assumed to be 1, and the cosmic background temperature T_{bg} is taken as 2.732 K. With the ^{12}CO ($J=2-1$) line properties listed in Table 1, we derive a CO column density of $4.0\times10^{16}\,\mathrm{cm}^{-2}$ for position A, and $1.9\times10^{16}\,\mathrm{cm}^{-2}$ for position B. Because ^{12}CO ($J=2-1$) is always considered optically thick, the column density derived here should be a lower limit. Compared with the column densities from LVG analysis, we find that LVG results at position A roughly agree with the LTE calculation, but for position B, all the LVG solutions are lower than the LTE lower limit. This result agrees with the scenario that at position B the LVG calculation requires less column density than LTE to explain the observing results because it takes into account enhanced photon escape probability due to a greater velocity gradient at the bright rim, where the nearby HII region agitates the molecular cloud with strong FUV radiation pressure and heating, exhibiting a case of RDI.

5 SUMMARY

We present an analysis of large scale mapping observations of the molecular lines ^{12}CO ($J=2-1$), ^{12}CO ($J=3-2$) , ^{13}CO ($J=2-1$) and ^{13}CO ($J=3-2$) transition emissions toward the Cepheus B molecular cloud. The target lies at the edge of the HII region S155, and is surrounded by an optically bright rim. The CO $J=3-2$ emission is stronger than the $J=2-1$ emission along the bright rim. PV diagrams of this region show a velocity gradient from the head of the cloud to the tail, which is characteristic of RDI. According to the LVG analysis, the density and temperature at the edge of the cloud are higher than that at the center. All of our results provide evidences that RDI is taking place in the Cepheus B molecular cloud.

Acknowledgements We would like to thank Sheng-Li Qin, Martin Miller and Nimei Chen for their permission to use observation data and for useful directions and discussions. We would also like to thank Rui Xue for his kind and helpful advice.

References

Bachiller, R., Fuente, A., & Kumar, M. 2002, A&A, 381,168
Bertoldi, F. 1989, ApJ, 346, 735
Beuther, H., Kramer, C., Deiss, B., & Stutzki, J. 2000, A&A, 362, 1109
Blaauw, A. 1964, ARA&A, 2, 213
Downes, D. 1989, in Evolution of Galaxies, Astronomical Observations, eds. I. Appenzeller, H. J. Habing & P. Lena (Heidelberg: Springer Verlag)
Felli, M., Tofani, G., Harten, R. H., & Panagia, N. 1978, A&A, 69, 199
Lefloch, B., & Lazareff, B. 1994, A&A, 289, 559
Lefloch, B., & Lazareff, B. 1995, A&A, 301, 522
Garden, P. R., Hayashi, M., Hasegawa, T., Gatley, I., & Kaifu, N. 1991, ApJ, 374, 540
Garmany, C. 1973, AJ, 78, 185
Getman, K., Feigelson, E., Luhman, K., Sicilia-Aguilar, A., Wang, J., & Garmire, G. 2009, ApJ, 699, 1454
Goldreich, P., & Kwan, J. 1974, ApJ, 189, 441
Minchin, N., Ward-Thomson, D., & White, G. 1992, A&A265, 733
Mookerjea, B., Kramer, C., Roellig, M., & Masur, M. 2006, A&A, 456, 235
Panagia, N., & Thum, C. 1981, A&A, 98, 295
Qin, S.-L., Zhao, J.-H., Moran, J. M., Marrone, D. P., Patel, N. A., Wang, J.-J., Liu, S.-Y., & Kuan, Y.-J. 2008a, ApJ, 677, 353
Qin, S.-L., Wang, J.-J., Zhao, G., Miller, M., & Zhao, J.-H. 2008b, A&A, 484, 361
Reipurth, B. 1983, A&A, 117, 183
Sargent, A. I. 1977, ApJ, 218, 736
Sargent, A. I. 1979, ApJ, 233, 163
Sharpless, S. 1959, ApJS, 4, 257
Sugitani, K., Morita, K., Nakano, M., Tamura, M., & Ogura, K. 1997, ApJ, 486, L141
White, G., Lefloch, B., Fridlund, C. Aspin, C., Dahmen, G., Minchin, N., & Huldtgren, M. 1997, A&A, 323, 931